FOI-R--0447--SE
March 2002
ISSN 1650-1942
Methodology report

Martin Nilsson

Dynamic Hardness Testing using a Split Hopkinson Pressure Bar Apparatus

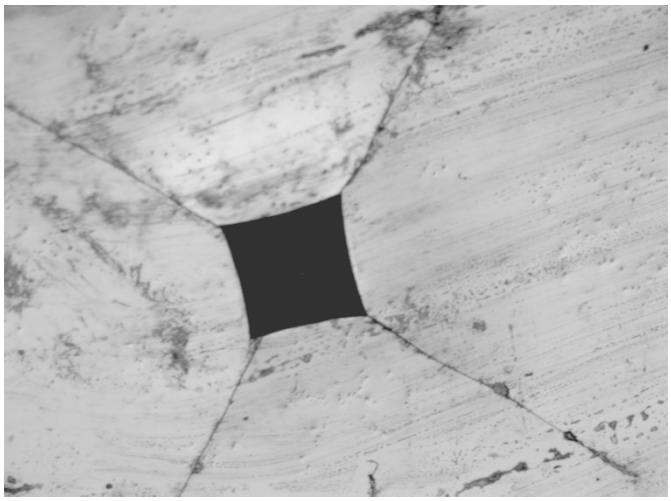

Weapons and Protection
SE-147 25 Tumba

SWEDISH DEFENCE RESEARCH AGENCY

Weapons and Protection
SE-147 25 Tumba

FOI-R--0447--SE

March 2002

ISSN 1650-1942

Methodology report

Martin Nilsson

Dynamic Hardness Testing using a Split Hopkinson Pressure Bar Apparatus

Intentionally left blank

Summary

To provide high strain and high strain rate data for new materials it is necessary to develop new and better testing methods. Indentation offers an attractive method because of ease of use, low costs, low material consumption and simple manufacturing of samples.

The goal of this work has been to develop a dynamic, hardness-testing device using elastic waves for loading and elastic wave theory for measurement.

The materials tested are 7075-T6 aluminium, SIS 2541-03 steel and SiAlON.

The set-up is similar to a traditional Hopkinson Pressure Bar. A projectile is propelled on to the transmitter bar by an air gun. The force acting on the indenter diamond and the indentation depth is calculated using the two strain method for non-uniform bars.

The experiments show that it is possible to measure hardness of metals and ceramics and fracture toughness of ceramics at higher strain rates with the apparatus. However, no definite conclusions can be made concerning the hardness of the materials tested. The number of samples is too small and the method has to be further evaluated.

The calculated permanent indentation depth is, in most cases, lower than the measured permanent indentation depth. Otherwise, the curves are correct in the sense that the loading phase is overlapping for different loads and the indentation is always recovering elastically with a similar slope when the applied load is declining.

Intentionally left blank

Contents

Intentionally left blank

1 Introduction

To provide high strain and high strain rate data for new materials there is a need to develop new and better testing methods. Indentation offers an attractive method because of ease of use, low costs, low material consumption and simple manufacturing of samples. Especially for brittle materials, that have no tensile plastic strain, indentation is an interesting method.

An important tool in extracting material properties is instrumented indentation, where the load-displacement curve is recorded during the test. Apart from hardness, and for brittle materials fracture toughness, indentation can also be used to obtain other elastic and plastic materials properties as described by Giannokopoulus et al. [1-7] and Milman et al. [8-11]. For further examples on instrumented indentation, see Öberg et al. [12] and Zeng et al. [5]. Instrumented indentation is required in the universal hardness standard DIN 50359 [13].

In previous work on dynamic hardness, Subhash et al. [14-17] used a Hopkinson bar to provided the dynamic load but wave theory was not used for force and displacement measurements. The goal of this work has been to develop a dynamic, instrumented hardness-testing device using elastic waves for loading and elastic wave theory for measurement.

2 Material

The materials tested are a 7075-T6 aluminium alloy, SIS 2541-03 steel and SiAlON containing 20 vol. % glass phase. The SiAlON is designated G20B06 and is described in detail by Petterson et al. [18]. The samples were approximately ∅10 by 3 mm and glued to the receiver bar using thermoplastic glue.

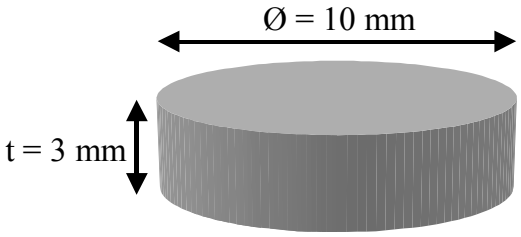

Figure 1. Dimensions of the samples.

3 Dynamic indentation set-up

The set-up is similar to an ordinary SHPB (Split Hopkinson Pressure Bar). A projectile is propelled on to the transmitter bar by an air gun. The force acting on the indentor diamond and the indentation depth is calculated using the two-strain method for uniform and non-uniform bars developed by Lundberg and Henchoz [19] and Lundberg et al. [20]. The calculations are described in chapter 4. The sample is connected to a receiver bar long enough to avoid reflections from its free end during the course of the experiment. Two pairs of strain gauges are glued to the transmitter bar at cross sections *A* and *B* and one pair of strain gauges is glued to the receiver bar at cross section *C*. The signals are stored on a transient recorder at a sampling rate of 1 MS/s (sample numbers > 1000) or 10 MS/s (sample numbers < 100).

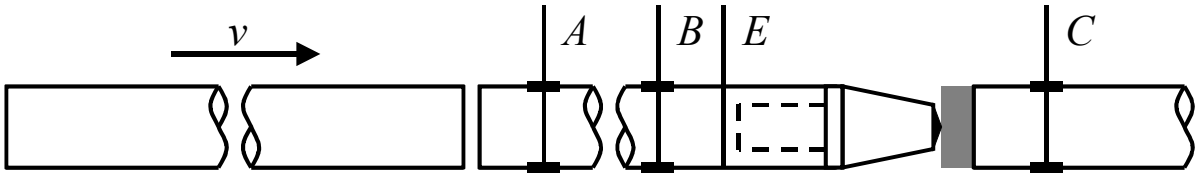

Figure 2. Set-up: projectile, transmitter bar, indentor, sample and receiver bar and the cross-sections where the strain is recorded (*A*, *B* and *C*) and evaluated (*E*).

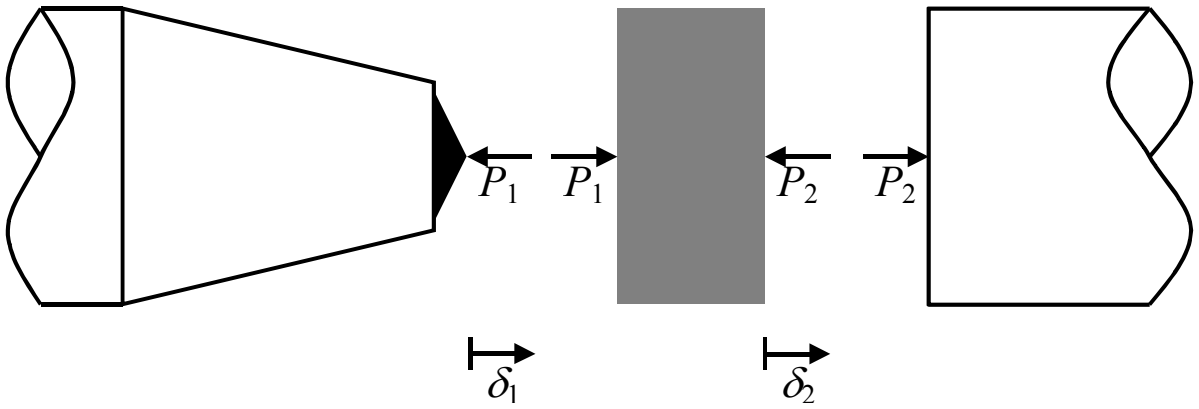

Figure 3. Forces acting at the interfaces between the indentor and the sample and the sample and the receiver bar (P_1 and P_2) and the displacement of the indentor and the sample back-plane (δ_1 and δ_2).

4 Two-strain method calculations

The two-strain method allows the analysis of overlapping elastic waves. The method is described in detail by Lundberg and Henchoz [19] for the case of uniform rods and Lundberg et al. [20] for non-uniform rods. Below, the solution is limited to constant elastic modulus and density and thereby constant elastic wave velocity and impedance.

The strain is measured at two points, *A* and *B*, and evaluated at a third cross-section, *E*. The analysis consists of solving time-domain difference equations. In the rod section *A*-*B*-*E*, the cross-section is uniform.

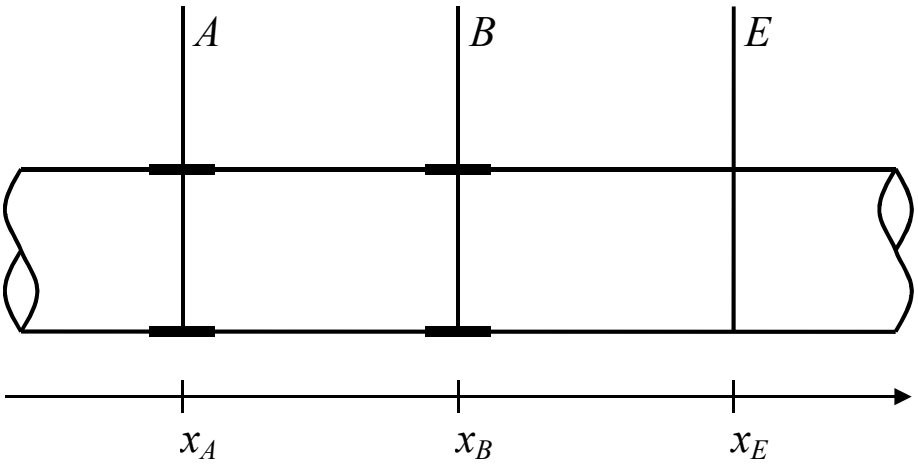

Figure 4. Uniform rod with three cross-sections *A*, *B* and *E*. The strain is measured in cross-sections *A* and *B* and evaluated in cross-section *E* [19].

The measured strains ε_A and ε_B relates to the strain waves in cross-section *E* travelling in the positive direction ε_E^P and negative direction ε_E^N and the total strain ε_E as:

$$\varepsilon_E^P(t) = \varepsilon_A(t - T_{AE}) - \varepsilon_B(t + T_{BE} - 2T_{AE}) + \varepsilon_E^P(t - 2T_{AB}) \tag{1}$$

$$\varepsilon_E^N(t) = \varepsilon_B(t + T_{BE}) - \varepsilon_A(t - T_{AE} + 2T_{BE}) + \varepsilon_E^N(t - 2T_{AB}) \tag{2}$$

$$\begin{aligned}\varepsilon_E(t) = {} & \varepsilon_A(t - T_{AE}) - \varepsilon_A(t - T_{AE} + 2T_{BE}) \\ & - \varepsilon_B(t + T_{BE} - 2T_{AE}) + \varepsilon_B(t + T_{BE}) + \varepsilon_E(t - 2T_{AB})\end{aligned} \tag{3}$$

Where

$$T_{AB} = \frac{x_B - x_A}{c} \qquad T_{AE} = \frac{x_E - x_A}{c} \qquad T_{BE} = \frac{x_E - x_B}{c} \tag{4}$$

In equation 4 $c = \sqrt{E/\rho}$ is the elastic wave speed and the x-coordinates are defined according to figure 4. Preferably, the times T_{AB}, T_{AE} and T_{BE} should be a multiple integer of the sampling step ΔT.

To get the force multiply the cross-section area by the elastic modulus and the strain:

$$P = AE\varepsilon$$

$$P_E^P(t) = P_A(t - T_{AE}) - P_B(t + T_{BE} - 2T_{AE}) + P_E^P(t - 2T_{AB}) \tag{5}$$

$$P_E^N(t) = P_B(t + T_{BE}) - P_A(t - T_{AE} + 2T_{BE}) + P_E^N(t - 2T_{AB}) \tag{6}$$

$$\begin{aligned} P_E(t) = {} & P_A(t - T_{AE}) - P_A(t - T_{AE} + 2T_{BE}) \\ & - P_B(t + T_{BE} - 2T_{AE}) + P_B(t + T_{BE}) + P_E(t - 2T_{AB}) \end{aligned} \tag{7}$$

The particle velocity at cross-section E is then given by:

$$v_E(t) = v_e(t - T_{AB}) + \frac{1}{Z_E}\left[-P_A(t) - P_A(t - 2T_{AB}) + 2P_B(t - T_{AB})\right] \tag{8}$$

Where Z_E is the characteristic impedance of the rod at cross-section E.

To be able to measure force and particle speed at the diamond interface, the non-uniform part of the rod, figure 2 and figure 3, has to be taken into account. The characteristic impedance of the rod is replaced by a piece-wise constant characteristic impedance Z_j for each piece, figure 5, with length Δx_j and transfer time T_j. The length of each piece Δx_j should be a multiple integer, m, of the elastic wave speed c times the sampling step ΔT.

$$T_j = \frac{\Delta x_j}{c} \qquad \Delta x_j = mc\Delta T \tag{9}$$

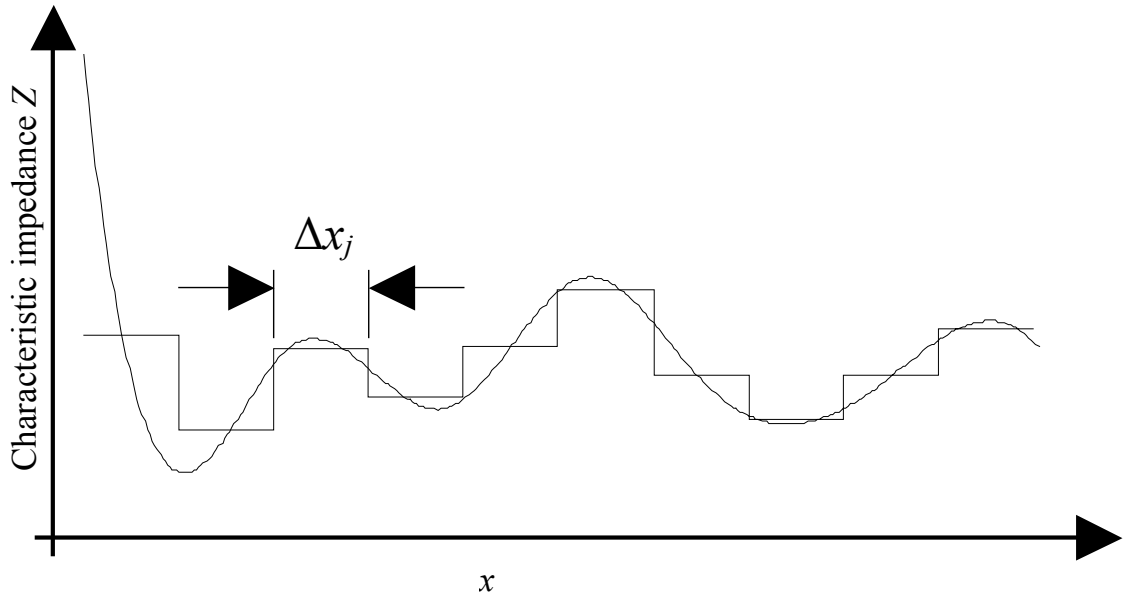

Figure 5. An example of the methodology, the characteristic impedance of the rod is replaced by a piece-wise constant characteristic impedance [20].

For each consecutive step Δx_j located between cross-section E and the indentor the force and velocity is calculated as:

$$P_j(t) = \frac{1}{2}\left[P_{j-1}(t+T_j) + P_{j-1}(t-T_j)\right] + \frac{Z_j}{2}\left[v_{j-1}(t+T_j) - v_{j-1}(t-T_j)\right] \tag{10}$$

$$v_j(t) = \frac{1}{2}\left[v_{j-1}(t+T_j) + v_{j-1}(t-T_j)\right] + \frac{1}{2Z_j}\left[P_{j-1}(t+T_j) - P_{j-1}(t-T_j)\right] \tag{11}$$

Where Z_j is the piece-wise constant characteristic impedance of the bar in the section.

The motion of the indentor can be calculated as the time integral of the velocity:

$$\dot{\delta}_1(t) = v_1(t) \quad \Rightarrow \quad \delta_1(t) = \int_0^t v_1(t)dt \tag{12}$$

But since the sample is glued to the receiver bar and the receiver bar is elastically deformed the velocity and motion of the back-plane has to be calculated:

$$\dot{\delta}_2(t) = v_C(t-T_{2C}) = \varepsilon_C(t-T_{2C})c = \frac{P_C(t-T_{2C})}{A_2 E}c \Rightarrow$$

$$\delta_2(t) = \frac{c}{A_2 E}\int_0^t P_C(t-T_{1C}) \tag{13}$$

Where ε_C is the strain at cross section C, c is the elastic wave speed, P_C is the force at cross section C, A_2 is the cross section area of the receiver bar, E is the elastic modulus of the bar and T_{1C} is the transfer time from the indentor to cross-section C:

$$T_{1C} = \frac{x_C - x_1}{c} \tag{14}$$

Finally the indentation velocity, $\dot{\delta}$, and indentation depth, δ, can be calculated as:

$$\dot{\delta}(t) = \dot{\delta}_1(t) - \dot{\delta}_2(t) = v_1(t) - v_C(t-T_{1C}) = v_1(t) - \frac{P_C(t-T_{1C})}{A_2 E}c \tag{15}$$

$$\delta(t) = \delta_1(t) - \delta_2(t) = \int_0^t v_1(t) - v_C(t-T_{1C})dt = \int_0^t v_1(t)dt - \frac{c}{A_2 E}\int_0^t P_C(t-T_{1C})dt \tag{16}$$

5 Experimental

5.1 Calculations of hardness and fracture toughness

The Vickers hardness is calculated as the mean contact pressure, i.e. load divided by projected area:

$$HV = \frac{P}{A} = \frac{P}{2a^2} \tag{17}$$

Where P is the load and a is half the length of the diagonal of the square impression.

In the experiments using a steel cone with a top angle of 110° the hardness was also calculated as the mean contact pressure:

$$HSC = \frac{P}{A} = \frac{P}{\pi d^2/4} \tag{18}$$

Where d is the diameter of the circular indentation. The maximum force measured at cross-section C, marked in figure 2, was used for the hardness calculations equation 17.

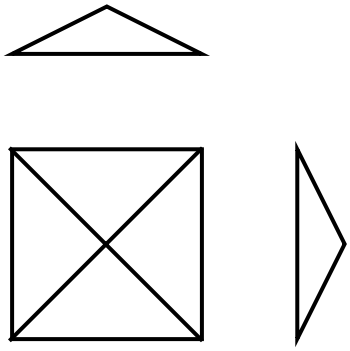

Figure 6. Vickers indentor. The indentor is pyramid shaped with a top angle of 136°.

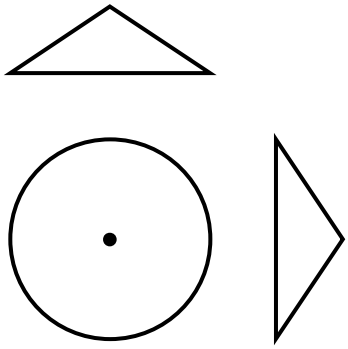

Figure 7. Cone shaped steel indentor. The indentor has a top angle of 110°.

To avoid border effects the thickness of the sample should be at least 10 times thicker than the indentation depth [13, 21]. This condition does only apply to the samples indented with the Vickers indentor.

For brittle materials, modus I fracture toughness, K_{IC}, can be calculated according to Anstis et al. [22]:

$$K_{IC} = 0.016\sqrt{\frac{E}{HV}}\frac{P}{c^{3/2}} \tag{19}$$

Where E is the Young modulus, HV is Vickers hardness according to equation 17, P is the load and c is the crack length from the impression centre, figure 8. The crack length used in equation 19 is the average of all four cracks originating from the indentation. The crack length is measured using a light optical microscope. The maximum force measured at cross-section *C*, marked in figure 2, was used for the fracture toughness, equation 19, calculations.

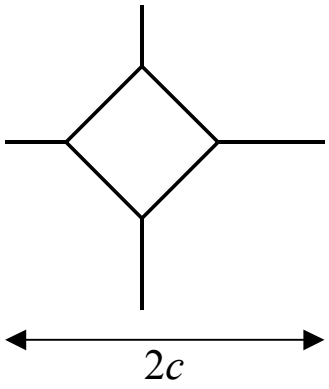

Figure 8. Crack length.

5.2 Results

A summary of the results regarding hardness from experiments using a Vickers indentor are shown in table 1 and figure 9-11 and regarding load-indentation curves in figure 13-16 and complete results are available in Appendix I (hardness and fracture toughness), Appendix II (load-indentation curves) and Appendix III (pictures of indentations). A summary of the experiments using a conical steel indentor is included in figure 9 and complete results are available in Appendix I (hardness) and Appendix II (load-indentation curves).

Quasistatic hardness and fracture toughness were measured or found in literature. It should be pointed out that in all cases the samples used for quasistatic and dynamic tests are the same.

Table 1. Comparison of quasistatic and dynamic indentation experiments.

Material		HV [GPa]	Std. Dev.	K_{IC} [MPa m$^{1/2}$]	Std. Dev.
Al 7075-T6	Quasistatic	1.21	0.02	–	–
	Dynamic	1.35	0.06	–	–
SIS 2541-03	Quasistatic	3.75	0.11	–	–
	Dynamic	3.62	0.07	–	–
SiAlON G20B06 [18]	Quasistatic [18]	15.8	–	5.3	–
	Dynamic	15.6	0.2	8.4	0.4

In figure 9 all the results from experiments on 7075-T6 aluminium are plotted as hardness against load. Apparently, in the case of the samples indented by a steel cone, the hardness is decreasing with increasing force. As mentioned above, in these experiments the indentation depth was more than 1/10 of the sample thickness, thereby not giving them a proper hardness value. The results from the quasistatic (■) and dynamic (▲) experiments with the Vickers indentor are included in figure 9 as comparison.

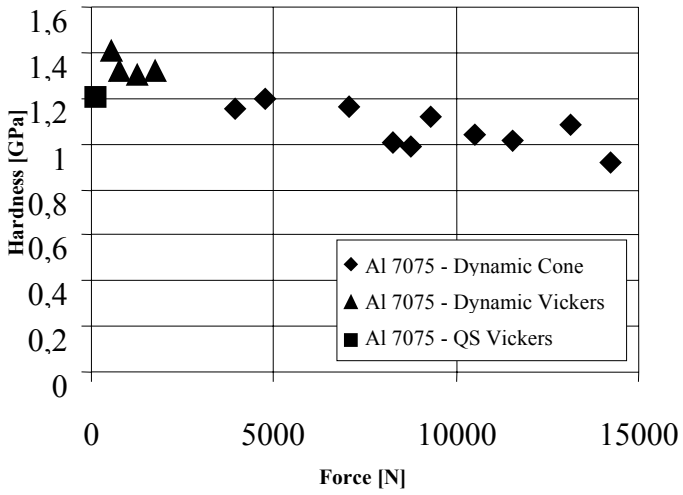

Figure 9. All tests performed on 7075-T6 aluminium alloy.

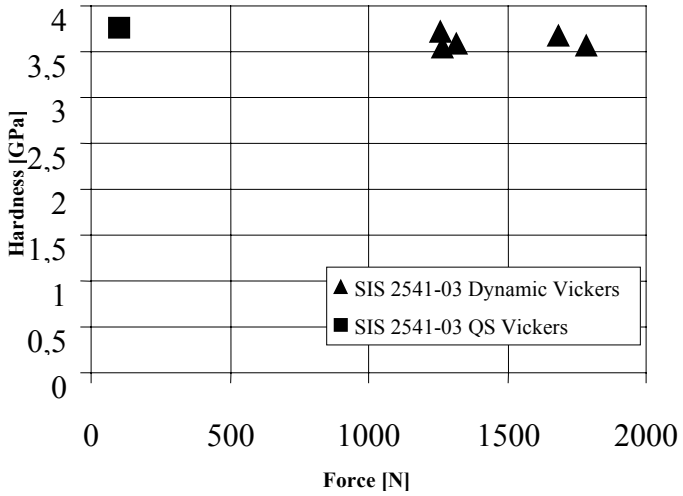

Figure 10. All tests performed on SIS 2541-03 steel.

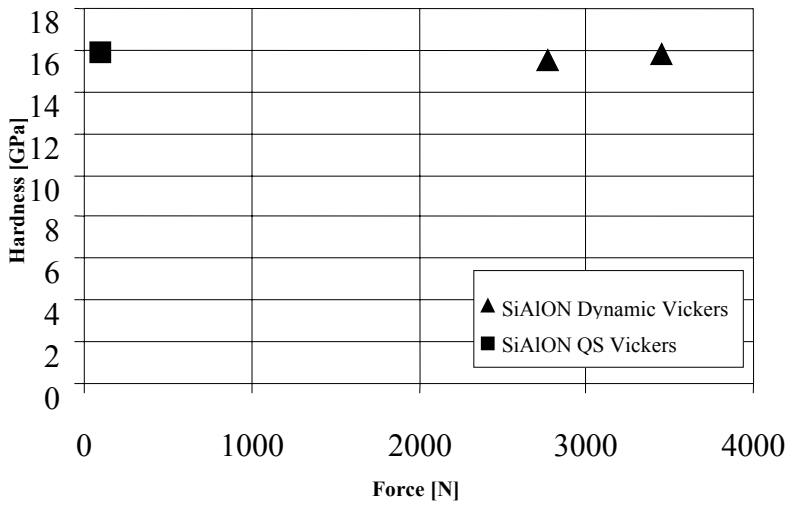

Figure 11. All tests performed on SiAlON.

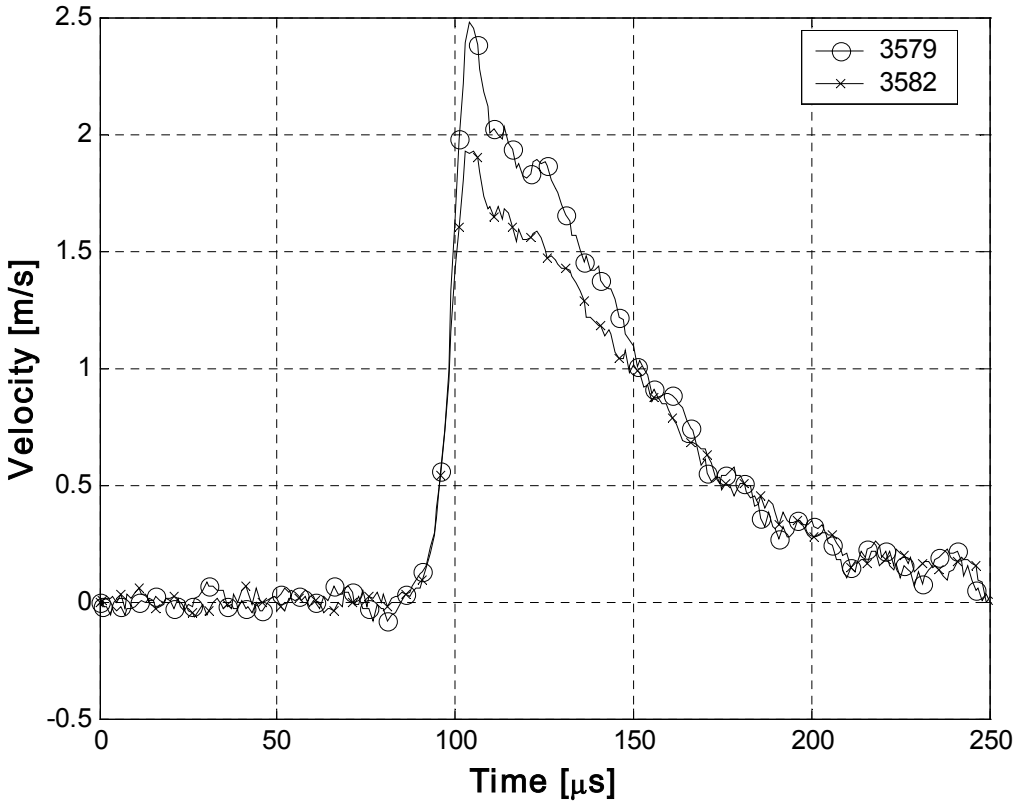

Figure 12. Indentation velocity during indentation of SiAlON.

Figure 12 shows the indentation velocity, δ, as described in equation 16, during indentation of SiAlON. The maximum velocity is about 2 m/s and decreases to 0 m/s after approximately 150 μm.

Calculations of load-indentation curves are found in chapter 4. Below, figure 13-16, there is a summary of all the load-indentation curves. Especially in the case of aluminium being indented by a steel cone, were 10 experiments are presented, it is clear that both loading and unloading phases are similar for all loads. Complete results are found in Appendix II.

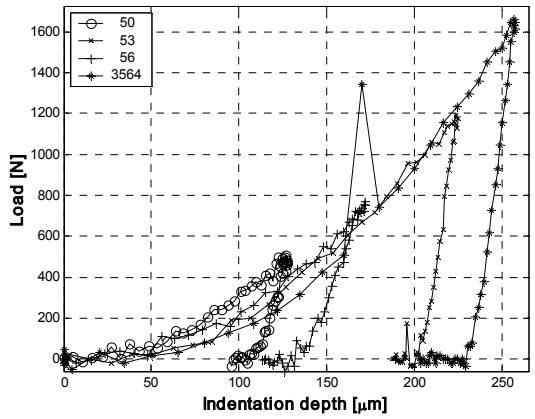

Figure 13. Load-indentation curves. Samples made of 7075-T6 aluminium indented by a Vickers indentor, top angle 136˚.

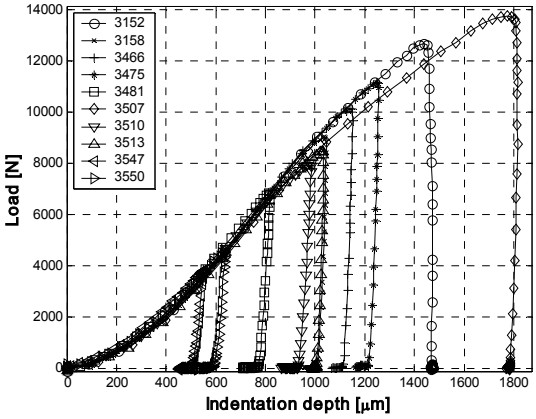

Figure 14. Load-indentation curves. Samples made of 7075-T6 aluminium indented by a steel cone with a top angle of 110˚.

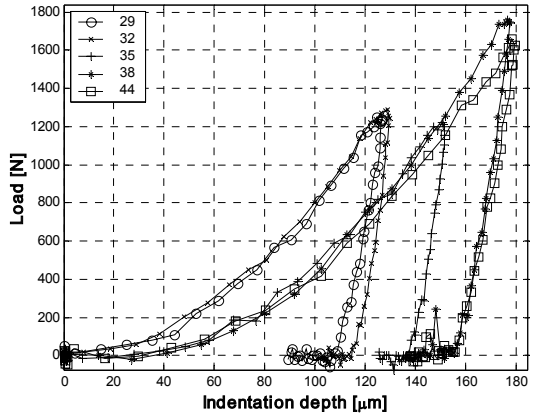

Figure 15. Load-indentation curves. Samples made of SIS 2541-03 steel indented by a Vickers indentor, top angle 136˚.

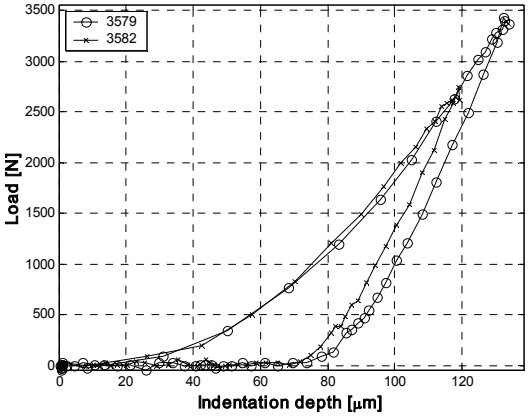

Figure 16. Load-indentation curves. Samples made of SiAlON indented by a Vickers indentor, top angle 136˚.

6 Discussion

6.1 Hardness

Since the analysis of the indentation process assumes quasistatic equilibrium it is important to make sure that this is valid. The sample has diameter of 10 mm and a thickness of 3 mm, thereby making the largest round-trip distance from the loaded centre to the edge 10 mm. The samples are loaded for approximately 200 μs, assuming the indentation depth does not grow when the load is declining. For aluminium and steel, the elastic wave speed is approximately 5000 m/s and for SiAlON the elastic wave speed is significantly higher. The number of round-trips that an elastic wave will make during the experiment is 5000 m/s*200 μs/10 mm = 100. The high number of round-trips makes sure that the system can be considered as in quasistatic equilibrium.

The experiments show that it is possible to measure hardness at higher strain rates with a SHPB apparatus. However, no definite conclusions can be made concerning the hardness of the materials tested. The number of samples is too small and the method has to be further developed and evaluated.

In the case of aluminium samples dynamically indented by a steel cone is it clear that the sample dimensions are too small. This is manifested by the loss of hardness at increasing loads.

6.2 Fracture toughness

Modus I fracture toughness, K_{IC}, presumes that the crack can be described with linear elastic fracture mechanics (LEFM). In brittle materials, like SiAlON, with low ductility and high yield stress, this is possible since the tensile plastic deformation can be neglected. Since the experiments here presented are dynamic it is necessary to make sure that the velocity of the crack propagation is not the limiting factor, i.e. the measured crack propagation velocity must be lower than the maximal possible crack propagation velocity. In the presented experiments, the cracks measure less than 1 mm and the load is applied for 200 μs, assuming no cracking occurs when the load is declining. This gives a measured crack propagation velocity of 1 mm/200 μs = 5 m/s. This means that the crack propagation is not a limiting factor since 5 m/s is orders of magnitude lower than the maximum crack propagation velocity.

The influence on the experimental results from stress waves in the sample also needs to be evaluated. The loading velocity during the experiments was, as highest, 2 m/s, and based on this low loading velocity it is assumed that the influence from stress waves in the sample can be neglected.

The experiments show that it is possible to measure fracture toughness of brittle materials at higher strain rates with a SHPB apparatus. However, based on a small number of samples, no conclusions about the fracture toughness of the SiAlON ceramic can be made. The number of samples is too small and it is possible that the length of the cracks was underestimated due to limitations of the light optical microscope.

6.3 Load-indentation depth

As seen in Appendix II the calculated permanent indentation depth is, in most cases, lower than the measured permanent indentation depth. Otherwise, the curves are correct in the sense

that the loading phase is overlapping for different loads and the indentation is always recovering elastically with a similar slope when the applied load is declining. There are several possible reasons why the calculations underestimate the indentation. An obvious source of error that is ignored in the model of the set-up is the threaded interface connecting the transmitter bar and the diamond indentor. The interface does not disturb the elastic wave propagation under pressure but it may disturb the propagation in tension. The interface may thereby act as a mechanism, trapping the wave in the indentor portion of the bar. Another source of error is the precision of establishing the distances between the cross-sections A and B and errors in the variations in characteristic impedance. An additional source of error is that the elastic deformation of the indentor is not taken into account.

7 Conclusions

The experiments show that it is possible to measure hardness and fracture toughness at higher strain rates with a SHPB apparatus.

The calculated permanent indentation depth is, in most cases, lower than the measured permanent indentation depth. Otherwise, the curves are correct in the sense that the loading phase is overlapping for different loads and the indentation is always recovering elastically with a similar slope when the applied load is declining.

Further work must focus on the underestimation of the indentation depth. In the continuation of the work, bars with smaller diameter should be used and the threaded interface between the transmitter bar and the indentor head should be eliminated.

Appendix I. Hardness and fracture toughness results

Table 2. Results from quasistatic hardness experiments on 7075-T6 aluminium indented by a Vickers indentor.

P [N]	$2a$ [mm]	HV [GPa]
98	0.4079	1.18
98	0.4039	1.20
98	0.4012	1.22
98	0.4010	1.22
98	0.4014	1.22
	Average:	1.21
	Std. Dev.:	0.02

Table 3. Results from dynamic hardness experiments on 7075-T6 aluminium indented by a Vickers indentor.

Sample	P [N]	$2a$ [mm]	δ [mm]	HV [GPa]
3564	1701	1.622	0.328	1.29
50	562	0.886	0.179	1.43
53	1266	1.382	0.279	1.33
56	804	1.097	0.222	1.34
			Average:	1.35
			Std Dev:	0.06

Table 4. Results from dynamic hardness experiments with samples made of 7075-T6 aluminium indented by a steel cone with a top angle of 110°.

Sample	*d* [mm]	δ [mm]	*P* [N]	*HSC* [GPa]
3152	3,930	1.376	13111	1.08
3158	3,252	1.139	9333	1.12
3466	3,580	1.253	10503	1.04
3475	3,815	1.336	11550	1.01
3481	2,782	0.974	7077	1.16
3507	4,441	1.555	14211	0.92
3510	3,232	1.131	8269	1.01
3513	3,363	1.178	8776	0.99
3547	2,083	0.729	3928	1.15
3550	2,255	0.789	4772	1.19

Table 5. Results from quasistatic hardness experiments on SIS 2541-03 steel indented by a Vickers indentor.

P [N]	*2a* [mm]	*HV* [GPa]
98	0.2285	3.76
98	0.2229	3.94
98	0.2330	3.61
98	0.2283	3.76
98	0.2299	3.74
98	0.2300	3.71
	Average:	3.75
	Std. Dev.:	0.11

Table 6. Results from dynamic hardness experiments on SIS 2541-03 steel indented by a Vickers indentor.

Sample	P [N]	$2a$ [mm]	δ [mm]	HV [GPa]
29	1264	0.8445	0.171	3.55
32	1320	0.8574	0.173	3.59
35	1256	0.8227	0.166	3.71
38	1786	0.9995	0.202	3.58
44	1686	0.9573	0.193	3.68
			Average:	3.62
			Std. Dev.:	0.07

Table 7. Results from dynamic hardness experiments on SiAlON indented by a Vickers indentor.

Sample	P [N]	$2a$ [mm]	δ [mm]	c [mm]	HV [GPa]	K_{IC} [MPa m$^{1/2}$]
3579	3455	0.662	0.134	0.9189	15.76	8.66
3582	2775	0.598	0.121	0.8361	15.52	8.07
				Average:	15.64	8.37
				Std. Dev.:	0.2	0.4

Appendix II. Load-indentation curves

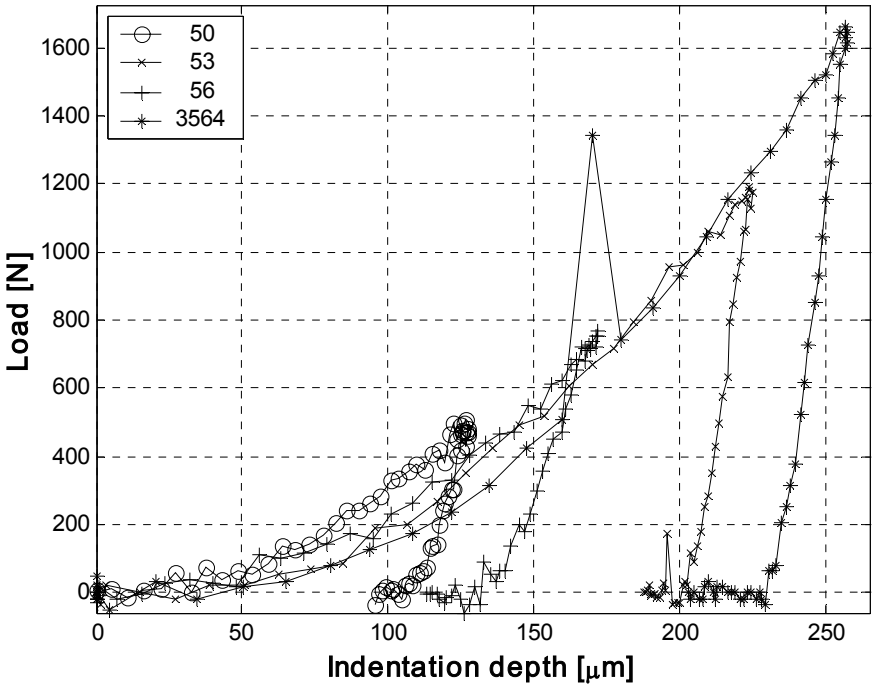

Figure 17. Load-indentation curves. All samples made of 7075-T6 aluminium indented by a Vickers indentor, top angle 136˚.

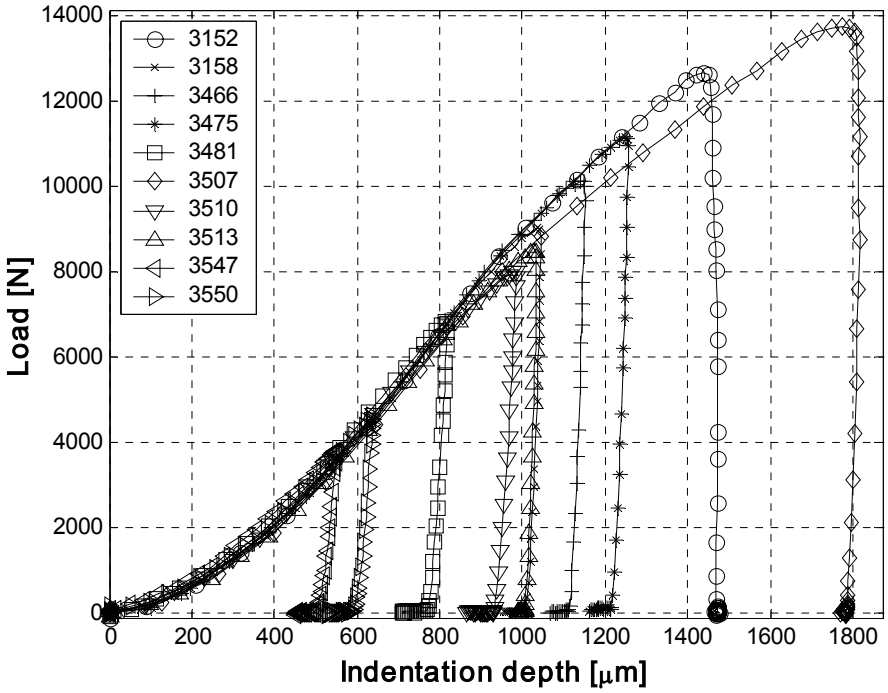

Figure 18. Load-indentation curves. All samples made of 7075-T6 aluminium indented by a steel cone with a top angle of 110˚.

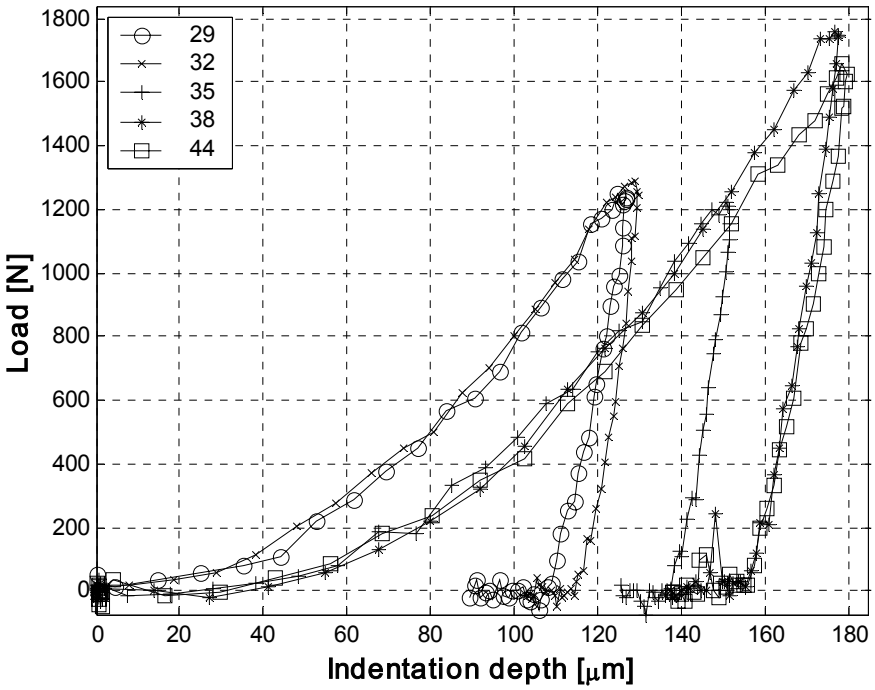

Figure 19. Load-indentation curves. All samples made of SIS 2541-03 steel indented by a Vickers indentor, top angle 136˚.

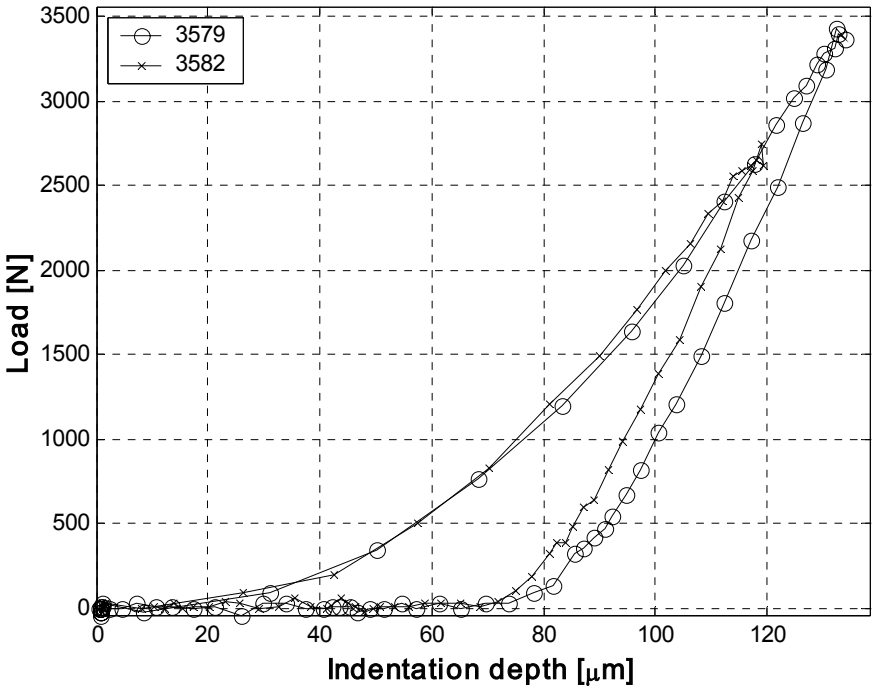

Figure 20. Load-indentation curves. All samples made of SiAlON indented by a Vickers indentor, top angle 136˚.

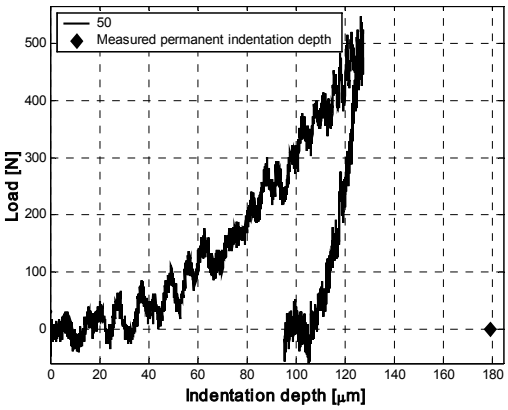

Figure 21. Load-indentation curve. Sample 50, 7075-T6 aluminium indented by a Vickers indentor.

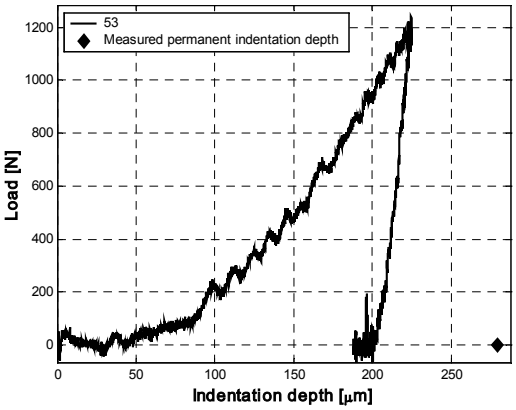

Figure 22. Load-indentation curve. Sample 53, 7075-T6 aluminium indented by a Vickers indentor.

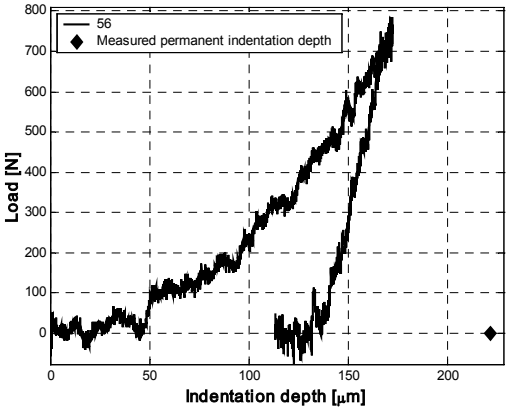

Figure 23. Load-indentation curve. Sample 56, 7075-T6 aluminium indented by a Vickers indentor.

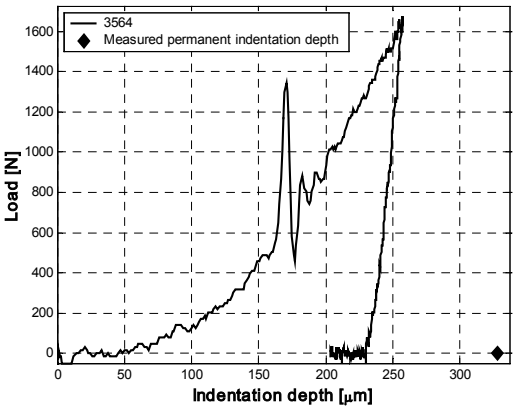

Figure 24. Load-indentation curve. Sample 3564, 7075-T6 aluminium indented by a Vickers indentor.

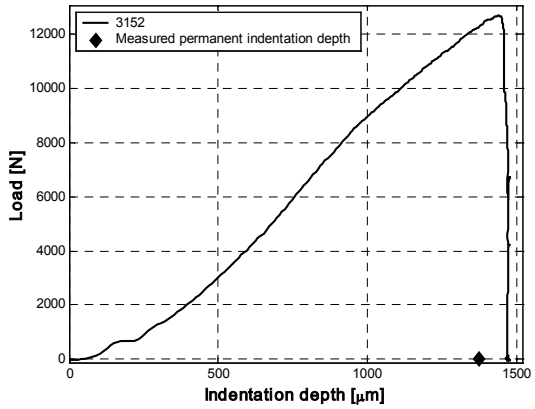

Figure 25. Load-indentation curve. Sample 3152, 7075-T6 aluminium indented by a steel cone.

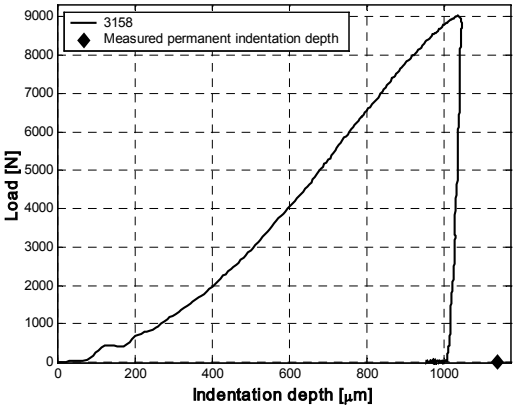

Figure 26. Load-indentation curve. Sample 3158, 7075-T6 aluminium indented by a steel cone.

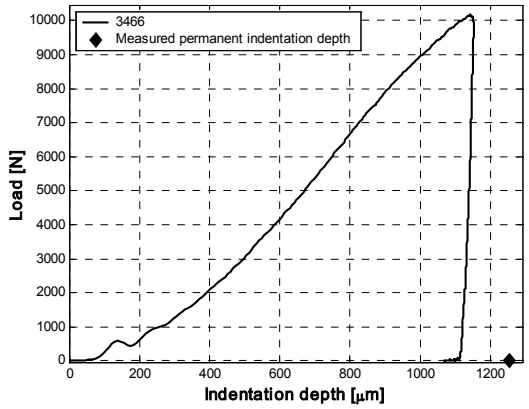

Figure 27. Load-indentation curve. Sample 3466, 7075-T6 aluminium indented by a steel cone.

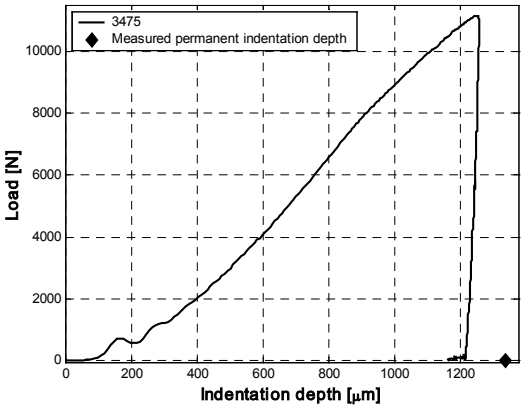

Figure 28. Load-indentation curve. Sample 3475, 7075-T6 aluminium indented by a steel cone.

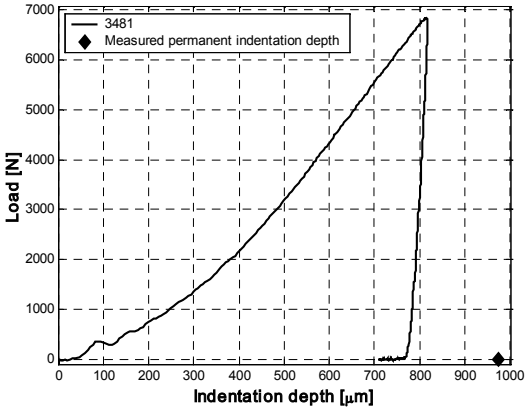

Figure 29. Load-indentation curve. Sample 3481, 7075-T6 aluminium indented by a steel cone.

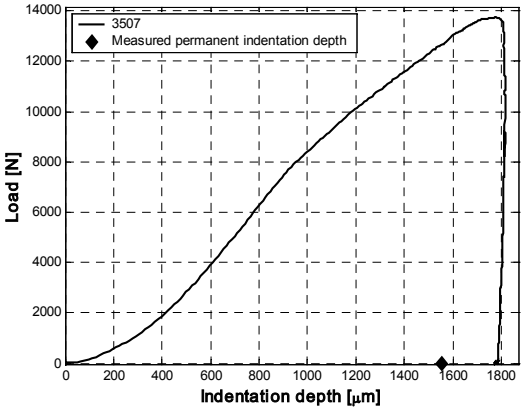

Figure 30. Load-indentation curve. Sample 3507, 7075-T6 aluminium indented by a steel cone.

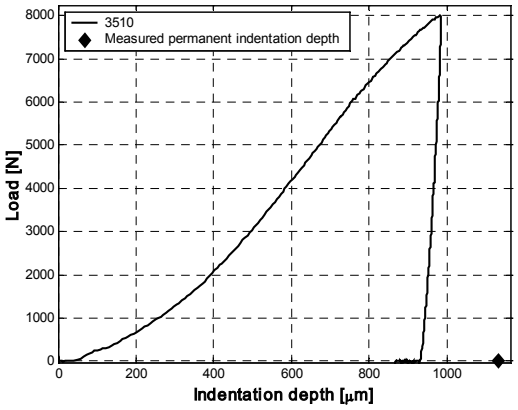

Figure 31. Load-indentation curve. Sample 3510, 7075-T6 aluminium indented by a steel cone.

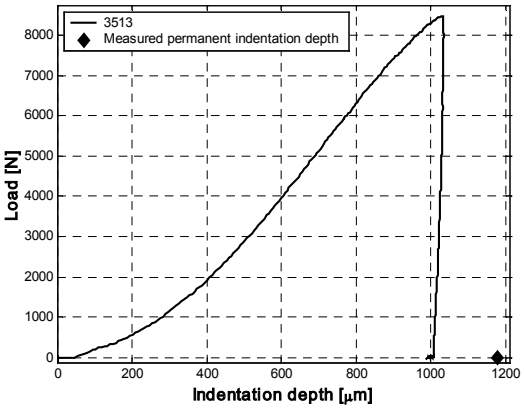

Figure 32. Load-indentation curve. Sample 3513, 7075-T6 aluminium indented by a steel cone.

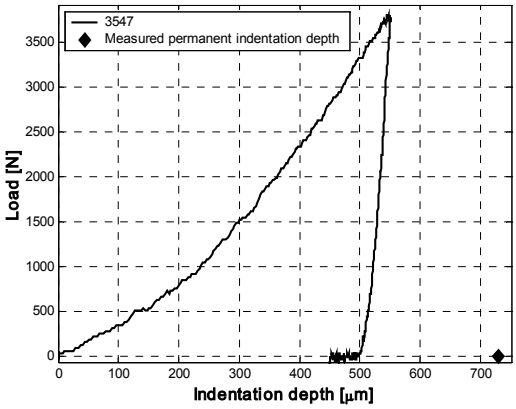

Figure 33. Load-indentation curve. Sample 3547, 7075-T6 aluminium indented by a steel cone.

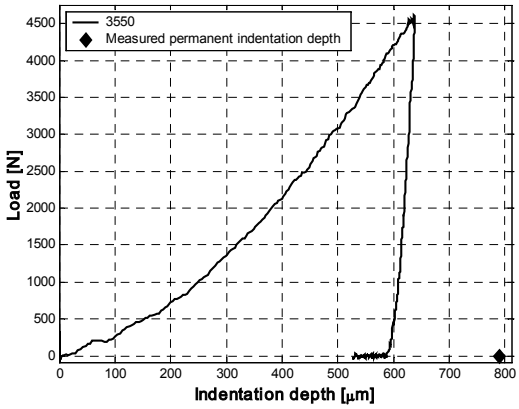

Figure 34. Load-indentation curve. Sample 3550, 7075-T6 aluminium indented by a steel cone.

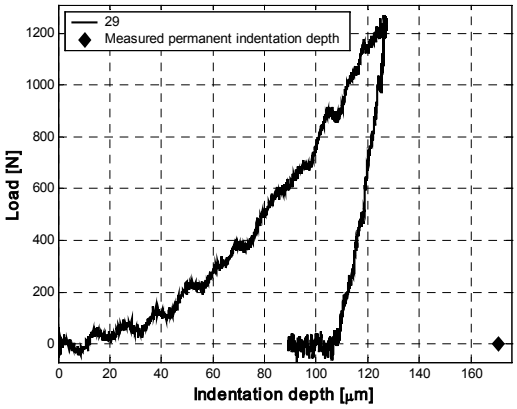

Figure 35. Load-indentation curve. Sample 29, SIS 2541-03 steel indented by a Vickers indentor.

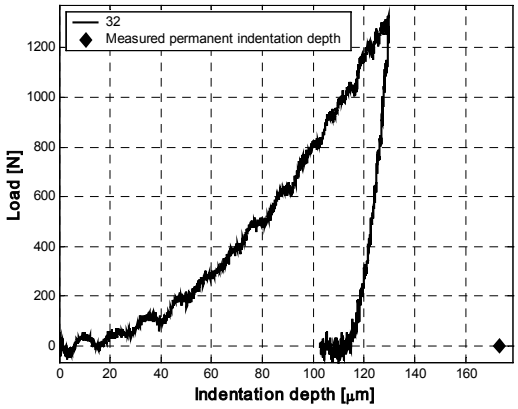

Figure 36. Load-indentation curve. Sample 32, SIS 2541-03 steel indented by a Vickers indentor.

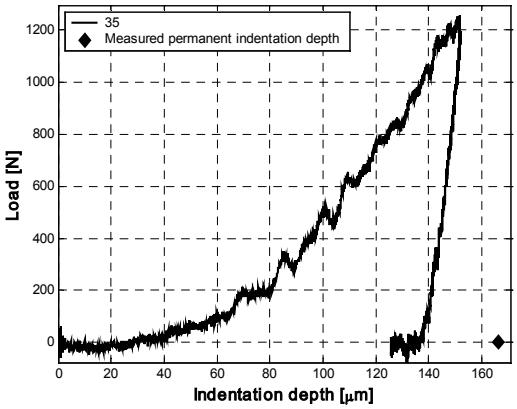

Figure 37. Load-indentation curve. Sample 35, SIS 2541-03 steel indented by a Vickers indentor.

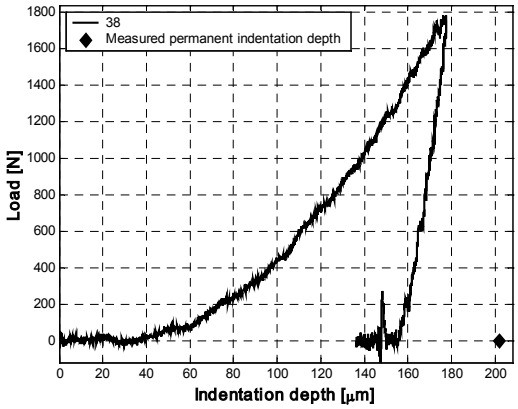

Figure 38. Load-indentation curve. Sample 38, SIS 2541-03 steel indented by a Vickers indentor.

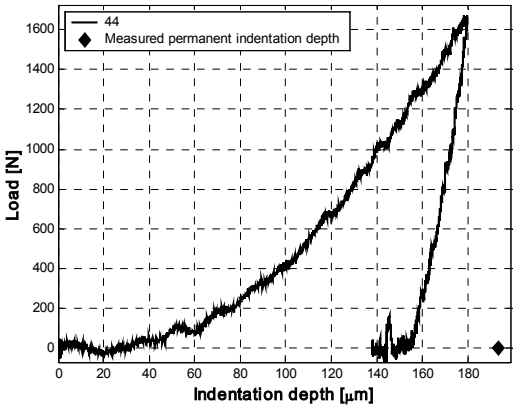

Figure 39. Load-indentation curve. Sample 44, SIS 2541-03 steel indented by a Vickers indentor.

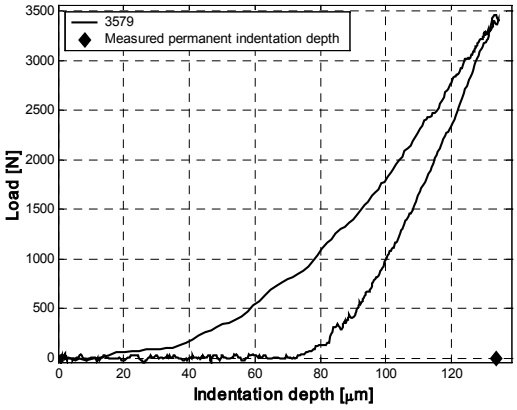

Figure 40. Load-indentation curve. Sample 3579, SiAlON indented by a Vickers indentor.

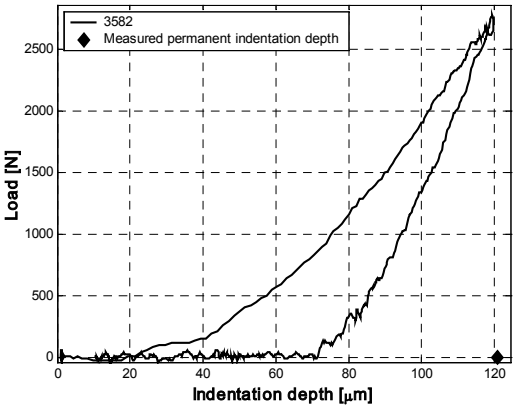

Figure 41. Load-indentation curve. Sample 3582, SiAlON indented by a Vickers indentor.

Appendix III. Pictures of indentations

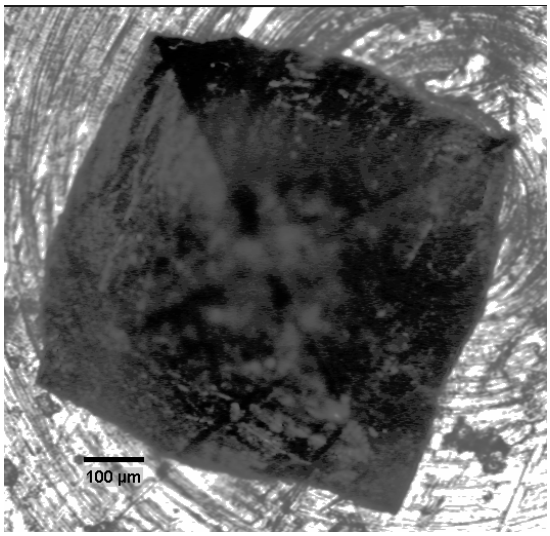

Figure 42. 7075-T6 aluminium, sample 50.

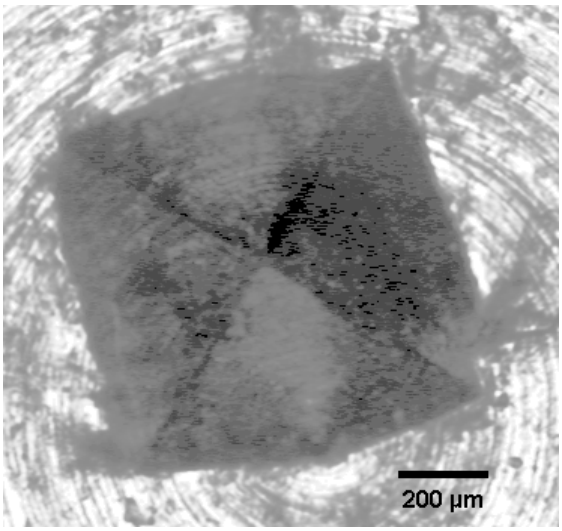

Figure 43. 7075-T6 aluminium, sample 3564.

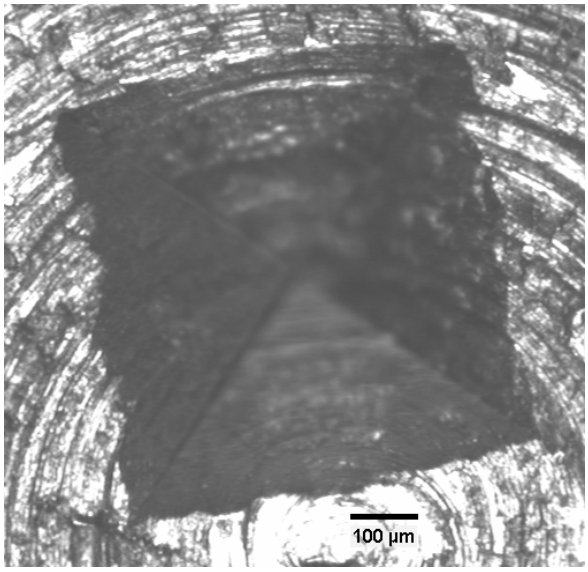

Figure 44. SIS 2541-03 steel, sample 29.

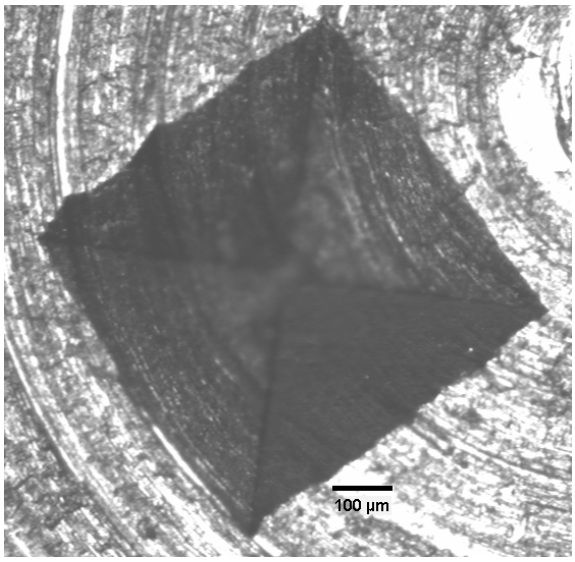

Figure 45. SIS 2541-03 steel, sample 32.

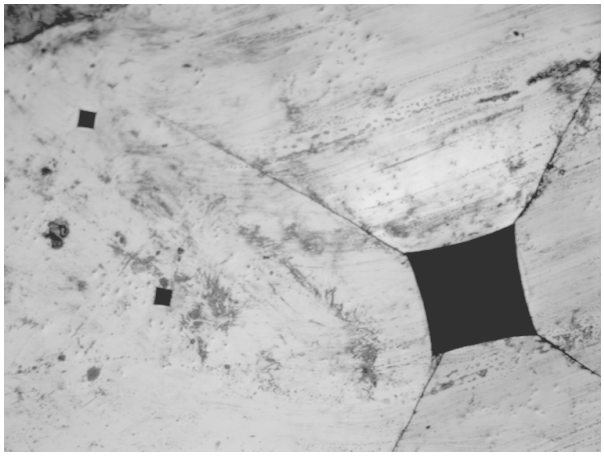

Figure 46. SiAlON G20B06 [18], sample 3579.

Figure 47. SiAlON G20B06 [18], sample 3579.

References

[1] A. E. Giannakopoulos and S. Suresh, “Determination of elastoplastic properties by instrumented sharp indentation”, *Scripta Materialia*, Vol. 40, p. 1191-1198, 1999.

[2] P.-L. Larsson, A. E. Giannakopoulos, E. Soderlund, D. J. Rowcliffe and R. Vestergaard, “Analysis of Berkovich indentation”, *International Journal of Rock Mechanics and Mining Science & Geomechanics Abstracts*, Vol. 33, p. 155A, 1996.

[3] P.-L. Larsson and A. E. Giannakopoulos, “Tensile stresses and their implication to cracking at pyramid indentation of pressure-sensitive hard metals and ceramics”, *Materials Science and Engineering A*, Vol. 254, p. 268-281, 1998.

[4] T. A. Venkatesh, K. J. Van Vliet, A. E. Giannakopoulos and S. Suresh, “Determination of elasto-plastic properties by instrumented sharp indentation: guidelines for property extraction”, *Scripta Materialia*, Vol. 42, p. 833-839, 2000.

[5] K. Zeng, E. Soderlund, A. E. Giannakopoulos and D. J. Rowcliffe, “Controlled indentation: a general approach to determine mechanical properties of brittle materials”, *Acta Materialia*, Vol. 44, p. 1127-1141, 1996.

[6] A. E. Giannakopoulos, P.-L. Larsson and R. Vestergaard, “Analysis of Vickers Indentation”, *International Journal of Solids and Structures*, Vol. 31, p. 2979-2708, 1994.

[7] A. E. Giannakopoulos and P.-L. Larsson, “Analysis of pyramid indentation of pressure-sensitive hard metals and ceramics”, *Mechanics of Materials*, Vol. 25, p. 1-35, 1997.

[8] Y. V. Milman, B. A. Galanov and S. I. Chugunova, “Plasticity Characteristic Obtained through Hardness Measurement”, *Acta Metallurgica et Materialia*, Vol. 41, p. 2523-2532, 1993.

[9] Y. V. Milman, S. I. Chugunova, I. V. Goncharova and S. Luyckx, “Determination of Ductility and Stress Strain Curve of WC Based Hard Metals by Indentation Method”, *Science of Sintering*, Vol. 29, p. 155-161, 1997.

[10] Y. V. Milman and S. I. Chugunova, “Mechanical Properties, Indentation and Dynamic Yield Stress of Ceramic Targets”, *International Journal of Impact Engineering*, Vol. 23, p. 629-638, 1999.

[11] Y. V. Milman, “Physics of the Hardness of Materials. New Possibilities of the Indentation Technique” presented at Sintering, 2000.

[12] H. Öberg, P.-L. Larsson and O. Magnius, “An Instrumented Microindentation Testing Device”, *Journal of testing and evaluation*, Vol. 29, p. 50-59, 2001.

[13] DIN 50359-1, “Universal hardness test. Part 1: Test method”.

[14] B. J. Koeppel and G. Subhash, “Experimental technique to investigate the dynamic indentation hardness of materials”, *Experimental Techniques*, Vol. 21, p. 16-18, 1997.

[15] B. J. Koeppel and G. Subhash, “Characteristics of residual plastic zone under static and dynamic Vickers indentations”, *Wear*, Vol. 224, p. 56-67, 1999.

[16] G. Subhash, B. J. Koeppel and A. Chandra, “Dynamic indentation hardness and rate sensitivity in metals”, *Journal of Engineering Materials and Technology, Transactions of the ASME*, Vol. 121, p. 257-263, 1999.

[17] R. J. Anton and G. Subhash, “Dynamic Vickers indentation of brittle materials”, *Wear*, Vol. 239, p. 27-35, 2000.

[18] P. Pettersson, M. Johnsson and Z. Shen, “Parameters for measuring the thermal shock of ceramic materials with an indentation-quench method”, *Journal of the European Ceramic Society*, In Press, Uncorrected Proof.

[19] B. Lundberg and A. Henchoz, “Analysis of elastic waves from two-point strain measurements”, *Experimental Mechanics*, Vol. 17, p. 213-218, 1977.

[20] B. Lundberg, J. Carlsson and K. G. Sundin, “Analysis of elastic waves in non-uniform rods from two-point strain measurement”, *Journal of sound and vibration*, Vol. 137, p. 483-493, 1990.

[21] ASTM C1327-99, “Standard Test Method for Vickers Indentation Hardness of Advanced Ceramics”.

[22] G. R. Anstis, P. Chantikul, B. R. Lawn and D. B. Marshall, “A Critical Evalution of Indentation Techniques for Measuring Fracture Toughness: I, Direct Crack Measurements”, *Journal of the American Ceramic Society*, Vol. 64, p. 533-538, 1981.

Issuing organization	Report number, ISRN	Report type
FOI – Swedish Defence Research Agency Weapons and Protection SE-147 25 Tumba	FOI-R--0447--SE	Methodology report
	Research area code 5. Combat	
	Month year March 2002	**Project no.** I231
	Customers code 5. Commissioned Research	
	Sub area code 51. Weapons and Protection	

Author/s (editor/s)	Project manager
Martin Nilsson	Magnus Oskarsson
	Approved by
	Sponsoring agency
	Scientifically and technically responsible

Report title

Dynamic Hardness Testing using a Split Hopkinson Pressure Bar Apparatus

Abstract (not more than 200 words)

To provide high strain and high strain rate data for new materials it is necessary to develop new and better testing methods. Indentation offers an attractive method because of ease of use, low costs, low material consumption and simple manufacturing of samples. The goal of this work has been to develop a dynamic, hardness-testing device using elastic waves for loading and elastic wave theory for measurement. The materials tested are 7075-T6 aluminium, SIS 2541-03 steel and SiAlON. The set-up is similar to a traditional Hopkinson Pressure Bar. A projectile is propelled on to the transmitter bar by an air gun. The force acting on the indenter diamond and the indentation depth is calculated using the two strain method for non-uniform bars. The experiments show that it is possible to measure hardness of metals and ceramics and fracture toughness of ceramics at higher strain rates with the apparatus. However, no definite conclusions can be made concerning the hardness of the materials tested. The number of samples is too small and the method has to be further evaluated. The calculated permanent indentation depth is, in most cases, lower than the measured permanent indentation depth. Otherwise, the curves are correct in the sense that the loading phase is overlapping for different loads and the indentation is always recovering elastically with a similar slope when the applied load is declining.

Keywords

hardness; indentation; fracture toughness; elastic wave propagation; Hopkinson bars

Further bibliographic information	Language English
ISSN 1650-1942	**Pages** 35 p.
	Price acc. to pricelist

Utgivare	Rapportnummer, ISRN	Klassificering
Totalförsvarets Forskningsinstitut - FOI Vapen och skydd 147 25 Tumba	FOI-R--0447--SE	Metodrapport
	Forskningsområde 5. Bekämpning	
	Månad, år Mars 2002	**Projektnummer** I231
	Verksamhetsgren 5. Uppdragsfinansierad verksamhet	
	Delområde 51. VVS med styrda vapen	

Författare/redaktör	Projektledare
Martin Nilsson	Magnus Oskarsson
	Godkänd av
	Uppdragsgivare/kundbeteckning
	Tekniskt och/eller vetenskapligt ansvarig

Rapportens titel (i översättning)

Dynamisk hårdhetsprovning med tryckhopkinsonutrustning

Sammanfattning (högst 200 ord)

För att erhålla materialdata vid höga töjningar och töjningshastigheter för nya material är det nödvändigt att utveckla nya och bättre provningsmetoder. Indentering är ett lämplig metod på grund av enkel metodik, låga kostnader, liten materialförbrukning och enkel provkroppstillverkning. Målet med detta arbete är att utveckla en dynamisk instrumenterad hårdhetsprovningsutrustning där elastiska vågor används för att belasta proven och mäta inträngningsdjupet. De material som provades var 7075-T6-aluminium, SIS 2541-03-stål och SiAlON. Provuppställningen liknar en traditionell tryckhopkinson. En projektil skjuts mot sändarstången med tryckluft. Kraften och förskjutningen hos indentorn beräknas med hjälp av tvåpunktsmetoden för icke-likformiga stänger. Försöken visar att det är möjligt att mäta hårdhet hos metaller och keramer och brottseghet hos keramer vid högre töjningshastigheter med uppställningen. Dock går det inte att dra några definitiva slutsatser om hårdheten hos de provade materialen. Antalet prov är litet och metoden måste utvecklas ytterligare. Det beräknade permanenta intrycksdjupet är, i de flesta fall, lägre än det uppmätta. Kurvorna är korrekta i så måtto att pålastningsfasen för olika laster är densamma och att intrycket alltid återhämtar sig elastiskt på likartat sätt när den pålagda lasten sjunker.

Nyckelord

hårdhet; indentering; brottseghet; elastisk vågutbredning; hopkinsonstänger

Övriga bibliografiska uppgifter	Språk Engelska
ISSN 1650-1942	**Antal sidor:** 35 s.
Distribution enligt missiv	**Pris: Enligt prislista**